IEEE Access
Multidisciplinary | Rapid Review | Open Access Journal

Received March 16, 2020, accepted March 29, 2020, date of publication April 6, 2020, date of current version April 17, 2020.

Digital Object Identifier 10.1109/ACCESS.2020.2985929

Predicting Path Loss Distribution of an Area From Satellite Images Using Deep Learning

OMAR AHMADIEN, HASAN F. ATES, (Senior Member, IEEE), TUNCER BAYKAS, (Senior Member, IEEE), AND BAHADIR K. GUNTURK
School of Engineering and Natural Sciences, Istanbul Medipol University, 34810 Istanbul, Turkey
Corresponding author: Bahadir K. Gunturk (bkgunturk@medipol.edu.tr)

This work was supported by the TUBITAK under Grant 215E324.

ABSTRACT Path loss prediction is essential for network planning in any wireless communication system. For cellular networks, it is usually achieved through extensive received signal power measurements in the target area. When the 3D model of an area is available, ray tracing simulations can be utilized; however, an important drawback of such an approach is the high computational complexity of the simulations. In this paper, we present a fundamentally different approach for path loss distribution prediction directly from 2D satellite images based on deep convolutional neural networks. While training process is time consuming and completed offline, inference can be done in real time. Another advantage of the proposed approach is that 3D model of the area is not needed during inference since the network simply uses an image captured by an aerial vehicle or satellite as its input. Simulation results show that the path loss distribution can be accurately predicted for different communication frequencies and transmitter heights.

INDEX TERMS Path loss, deep learning, convolutional neural networks.

I. INTRODUCTION

For wireless communication system operators, estimating the path loss is necessary for network planning of the target coverage area. For small number of transmitter locations, outdoor field measurements can be done to obtain the channel parameters [1], [2]. Alternatively, with the aid of the 3D model of the area, ray tracing (RT) or ray launching (RL) simulations can be deployed. The performance of these methods is satisfactory when it is compared to the field measurements [3], [4]. RT and RL simulations require 3D models, which can be obtained in different ways, such as depth estimation from stereo image pairs. Nevertheless, 3D model of a target area may not be readily available, and generating one in a short time is neither economical nor practical. It should also be noted that, even when the 3D model is available, high computational costs of RT/RL simulations prevent real time applications [5], [6].

Various models have been suggested to estimate path loss for wireless communication networks. One of these models is the COST231 Walfisch-Ikegami (COST-WI) model, which is applicable for urban areas as it contains parameters like street orientations, road widths, separation between buildings, and heights of buildings [7]. Such detailed features of a region are usually hard to obtain, limiting the use of these models. Simpler models have also been proposed; for example, the model in [8] includes only the building density between the transmitter and receiver. Estimating the building density from images requires manual annotation or the use of computer vision based segmentation techniques [9], [10].

Machine learning techniques are increasingly utilized in wireless communication applications, including path loss prediction. For example, in [11], the use of artificial neural network (ANN), support vector machine (SVM), as well as dimensionality reduction techniques, is investigated to predict path loss. The features include building heights, widths and distances from the transmitter along the path between the transmitter and the receiver. The choice of feature set is critical; and various other features, such as transmitter/receiver heights, antenna seperation, transmitting frequency, mean building height and road width have been proposed [12]–[18]. Aside from urban areas, it is also possible to classify the target region from the aerial images into different classes such as forest or village, and use a suitable path loss model [19]. Recently in [20], a survey of existing machine learning methods in literature for path loss predic-

The associate editor coordinating the review of this manuscript and approving it for publication was Celimuge Wu.

tion, including decision tree based [21] and support vector regression based [22] methods, is presented. Moreover, the use of satellite images as input to a deep neural network is utilized in [23] to predict LTE signal quality metrics, including RSRP (Reference Signal Received Power), RSRQ (Reference Signal Received Quality) and SINR (Signal to Interference and Noise Ratio). In a recent study [24], deep learning model is applied on real measurements with the aid of satellite images and input features to predict the RSRP for specific receiver locations in a limited area/scenario. Instead, in [25], channel parameters (e.g., path loss exponent and standard deviation of shadowing) are estimated directly from satellite images using deep learning without the need of any additional input features and for different area types and scenarios.

In this paper, we present a deep learning based method to predict the distribution of path loss in a given region. This is unlike the existing approaches, which explicitly use 3D models (e.g., in [11]), 2D segmented images (e.g., in [9], [10]), or satellite images aided with additional features (e.g., in [23], [24]) to predict the path loss at a specific receiver location. For the first approach, it is necessary to have 3D models, which may not be available for a target region. For the second approach, the target region has to be segmented, which is done either manually (which is time consuming) or automatically (which is prone to error); moreover, the lack of height information (using only segmented images) limits the performance of segmentation based approaches. The approach in [24] is similar in spirit to ours that it uses deep learning and satellite images to predict path loss. However their application scenario is very limited, since all the training and test data come from the same university campus. Our dataset, on the other hand, covers different types of regions, such as densely populated urban/suburban regions, with or without high-rise buildings, vegetation, and water.

The proposed approach in this paper uses 2D aerial/satellite images directly, without any additional features, to estimate the path loss distribution of the whole area. While most of the existing work (e.g. [10], [24]) in literature aims to predict path loss at a single receiver location, our goal is to predict the distribution of path loss in the entire region. Path loss distribution depends mostly on the general characteristics of a region (i.e. urban/suburban region type, and the density of high-rise buildings, etc.). In this paper we also show that regions with similar characteristics have similar path loss histograms. Our deep learning model learns these regional characteristics from 2D cues in the satellite image and successfully predicts the corresponding path loss histogram.

Another advantage of the proposed approach is that the features are learned through deep learning, as opposed to manually crafting features, which takes time and effort, and is not guaranteed to depict the underlying characteristics affecting the prediction. Our deep learning based method uses a convolutional neural network (CNN), which incorporates multiple convolutional layers [26] for feature learning. We adapt a well-known CNN architecture, VGG-16 [27], for the problem of path loss distribution prediction. (The use of other deep architectures, such as ResNet [28], is possible but not investigated in this paper.)

Deep learning based methods have been used before in several other areas of telecommunications. For example, in [29] and [30], it is used to identify wireless technologies. In [31], cooperative spectrum sensing with ANN is developed. An important research field for new generation wireless networks is how to allocate resources between different users; in [32], it is suggested to use ANN for proactive resource allocation. In [33], an unsupervised learning based relay selection method is introduced for multi-hop networks.

The proposed approach uses 2D satellite images in path loss distribution prediction. This approach turns out to be successful because a satellite image includes low-level and high-level cues/features, such as color, shape, texture, shadows, non-orthogonal views of buildings, to help infer the 3D structure and 2D information (e.g., building and non-building areas), which are critical in the wireless channel characteristics. The optimal features are learned by the deep network through training. There are some recent studies demonstrating the use of deep networks to extract building segments [34], [35] and 3D structures [36] from 2D images; these studies also demonstrate the feasibility of extracting 3D characteristics of a region from 2D images.

In our case, the deep network takes a satellite image as its input, and produces the path loss distribution of the entire area at the output. The path loss distribution is quantized as a fixed-bin-size histogram; and the value of each bin is predicted using supervised regression. The regression network is based on the VGG-16 architecture, whose pre-trained weights are used for initialization before training. In a previous work [25], we also used deep learning for path loss model parameter prediction. The main difference between [25] and this work is that, in [25] we predict two model parameters, i.e. path loss exponent and shadowing factor. In this work, we predict the overall distribution of path loss. In [25], path loss exponent and shadowing factor parameters are quantized, forming a discrete set of classes; hence, the network is constructed as a classifier network. In this work, the path loss distribution is divided into bins to form a histogram; and the network is constructed as a regression network.

Our main contributions can be listed as follows:

- We show that deep learning can be used to accurately predict path loss distribution from 2D satellite images without the need for a 3D model of the region.
- Through transfer learning (i.e., using a pre-trained existing network architecture), we achieve good prediction performance even with a limited dataset.
- We show that a deep network model can be trained for any specific transmitter height and frequency. We compare the experimental results for multiple scenarios (i.e., different transmitter height and frequency combinations).

In Section II, we give an overview of the proposed approach. In Section III, we explain how the dataset (to be

used in training and testing the network) is generated. We give the details of the network in Section IV. We discuss the results in Section V and conclude the paper in Section VI.

II. OVERVIEW OF THE PROPOSED APPROACH

For a wireless communication system, the propagation path loss is defined as the power loss that happens in the channel between the transmitter and the receiver. Path loss is crucial in defining the channel characteristics, and for the design and analysis of wireless communication systems [37].

Path loss can be defined as the ratio between transmitted and received powers [38], and in logarithmic scale it can be written as:

$$PL = P_{T_x} - P_{R_x} \tag{1}$$

where PL is the path loss (in dB), P_{T_x} is the transmitted power, and P_{R_x} is the received power.

According to the log-normal shadowing model [37], the large-scale path loss can be modeled using the following formula:

$$PL(d) = PL(d_0) + 10n \log_{10}\left(\frac{d}{d_0}\right) + X_\sigma, \tag{2}$$

where $PL(d)$ is the path loss (in dB) at distance d from the transmitter, $PL(d_0)$ is the path loss at a reference distance d_0, n is the path loss exponent and X_σ is a normal random variable with zero mean and standard deviation of σ, *i.e.*, the large-scale shadowing factor which refers to the amount of shadowing in the environment. This model is widely used in communication systems, including air-to-ground UAV communications [39].

The goal of this work is to obtain the path loss characteristics in a region. Instead of the log-normal shadowing model given in (2), where the excessive path loss X_σ is modeled as a random variable, we assume the path loss PL is a random variable and estimate its distribution directly. Specifically, we propose a deep learning based method to estimate path loss distribution in an area using 2D aerial/satellite images of the area. This is illustrated in Fig. 1. The path loss distribution is modeled as a histogram with fixed bin locations and widths. The network consists of convolutional layers (to extract the features from the input image) and a regression layer to predict the value of each bin. The details of the network architecture will be discussed in Section IV.

III. DATASET GENERATION

Deep neural networks require large amount of data for training. For our task, it is not feasible to do actual measurements to cover a variety of scenarios. Therefore, we follow the process of using 3D models and ray tracing simulations to generate the dataset [25]. (While some parts of the process are identical to those of [25], we write all the steps here for completeness.) In Fig. 2, we present the dataset generation process. We acquire a set of images with corresponding 3D models. For an image, we use its 3D model in a ray tracing simulation to calculate the path loss at a dense grid of receiver locations. The path loss histogram is calculated for the entire region; and the image-histogram pair is added to the dataset. This process is repeated for all regions.

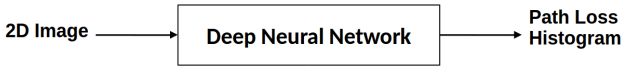

FIGURE 1. Path loss distribution prediction. An aerial/satellite image is input to a deep neural network to obtain an estimate of the path loss distribution for that region.

To obtain the 3D models and the corresponding satellite images, we use the SketchUp software[1] with the PlaceMaker plugin.[2] The area of each region is 1.8 × 1.8 km. We then use Wireless InSite software[3] to import each 3D model and do a ray tracing simulation. For the simulation, we use a flat terrain model and place a grid of 12,100 (110 × 110) receiver points and one transmitter point at the center of the 3D model. The receiver points are positioned at 1.5 meters from ground level. The receiver points that are inside the buildings are then excluded. Hence, only outdoor receiver locations are considered when computing the path loss histograms. The transmitting power is set to 60 dBm using an omni-directional antenna. The terrain material is set as dry earth while the buildings are set as concrete in the simulation environment. The simulations are repeated for different transmitter heights and frequencies, as shown in Table 1. The simulation parameters are summarized in Table 2.

TABLE 1. Transmitter heights and frequencies used to generate the datasets.

Frequency	Height
3.5 GHz	300 m
900 MHz	300 m
900 MHz	80 m

TABLE 2. Measurement parameters.

Transmission frequencies	900 MHz or 3.5 GHz
Transmit Power	+60 dBm
Antenna polarization	Vertical
Antenna radiation pattern	Omni-directional
Transmitter antenna height	300 m or 80 m
Receiver antenna height	1.5 m
Transmitted signal	Sinusoid
Bandwidth	8 MHz
d_0	57.28 m
$PL(d_0)$	63.44 dB

By quantizing the path loss values of the outdoor receivers, the path loss distribution is formed as an 8-bin

[1] https://www.sketchup.com/
[2] https://www.suplacemaker.com/
[3] https://www.remcom.com/wireless-insite-em-propagation-software

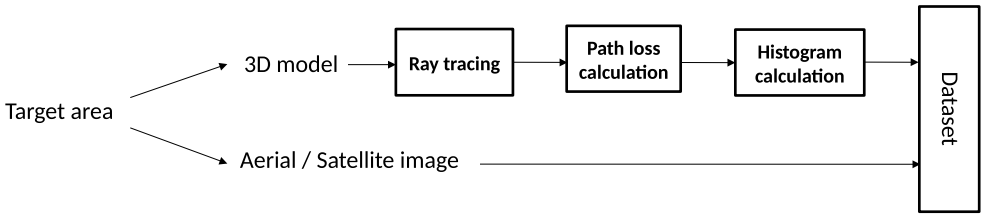

FIGURE 2. Dataset generation process. For a target area, we have both its satellite/aerial image and 3D model. The 3D model is first processed with ray tracing simulation to calculate the path loss at each receiver point; the path loss values are then used to calculate the path loss histogram of that region. The histogram and the corresponding image are added to the dataset.

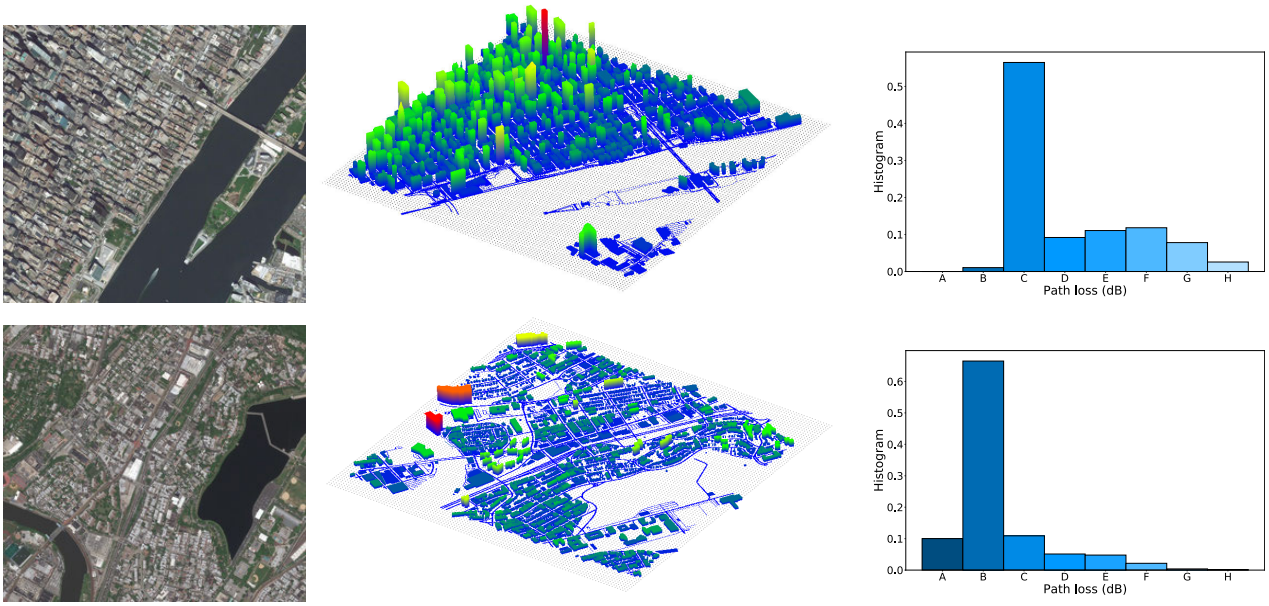

FIGURE 3. Satellite images, their corresponding 3D models, and path loss histograms are shown for two different regions. For the path loss bin ranges, refer to Table 3.

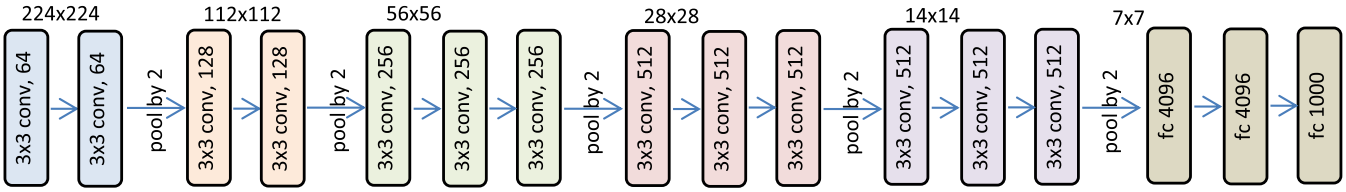

FIGURE 4. The VGG-16 architecture [27]. In this figure, "fc" stands for fully connected layer and "conv" stands for convolution layer. The last layer is changed in our method.

TABLE 3. Path loss (*PL*) bin values.

$PL(d_0) = 63.44\ dB$	
A	$PL - PL(d_0) \leq 20$
B	$20 < PL - PL(d_0) \leq 30$
C	$30 < PL - PL(d_0) \leq 40$
D	$40 < PL - PL(d_0) \leq 50$
E	$50 < PL - PL(d_0) \leq 60$
F	$60 < PL - PL(d_0) \leq 70$
G	$70 < PL - PL(d_0) \leq 80$
H	$80 < PL - PL(d_0)$

histogram. As shown in Table 3, the residual path loss, that is, the measured path loss minus the reference path loss, is split into 8 bins, with intermediate bin widths of 10 dB.

As a result, we obtain a total of three datasets, for three different height-frequency combinations as indicated in Table 1. Each dataset consists of 999 images with their corresponding path loss histograms. In Fig. 3, we provide two sample images, their corresponding 3D models, and the calculated path loss histogram. It should again be noted the 3D models are used in training or testing the network; they are only used to generate the histograms through ray tracing simulations. More samples are provided in Section V.

TABLE 4. Average and median MSE values between the true and predicted histograms.

	Proposed method		Baseline method		Variance of the dataset
Dataset	Average	Median	Average	Median	
3.5 GHz 300 m	0.0027	0.0001	0.0275	0.0260	0.0623
900 MHz 300 m	0.0003	0.0001	0.0224	0.0209	0.0618
900 MHz 80 m	0.0016	0.0003	0.0038	0.0023	0.0360

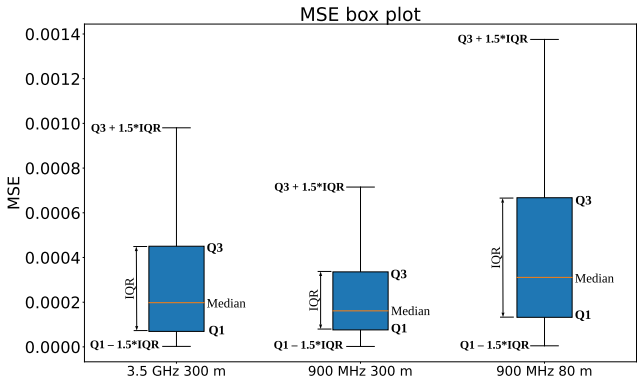

FIGURE 5. This box plot shows the distribution of the MSE based on the median, first quartile (Q1): the middle value between the smallest value and the median of the MSE dataset, third quartile (Q3): the middle value between the median and the highest value of the MSE dataset, interquartile range (IQR): 25th to the 75th percentile, maximum: (Q3 + 1.5*IQR), and minimum: (Q1 − 1.5*IQR).

IV. NETWORK ARCHITECTURE

Instead of training a network from scratch, we take a pre-trained network (trained for image classification), make the necessary modifications for our purpose, and fine-tune it with our training set. This idea of transfer learning is adopted when the size of the dataset is not large enough. Specifically, we utilize a well-known architecture, named VGG-16 [27]. VGG-16 is a network of medium depth, which has more than 138 million trainable parameters. The network is pre-trained using the 1000-class ILSVRC ImageNet dataset [40]. The VGG-16 architecture is shown in Fig. 4; we use the same architecture except for the last layer. The last layer is replaced with a fully connected layer of 8 outputs, corresponding to the bins of the path loss histograms; and finally, the softmax function is applied to outputs.

For optimization, the cross-entropy loss function is used. The network outputs (b_i) are mapped to probabilities using the softmax function and then the cross-entropy loss (L_{CE}) is computed:

$$L_{CE} = -\sum_{i=1}^{8} h_i \log(p_i), \quad \text{where } p_i = \frac{\exp(b_i)}{\sum_j \exp(b_j)} \tag{3}$$

and h_i are the true histogram values. The training process is explained in detail in the next section.

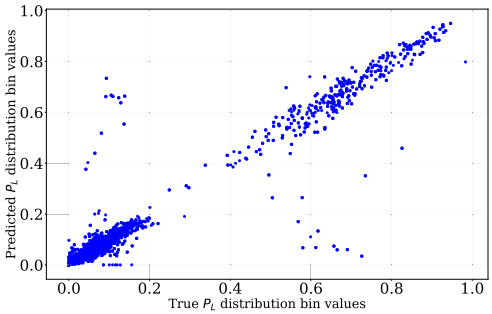

(a) 3.5 GHz 300 m.

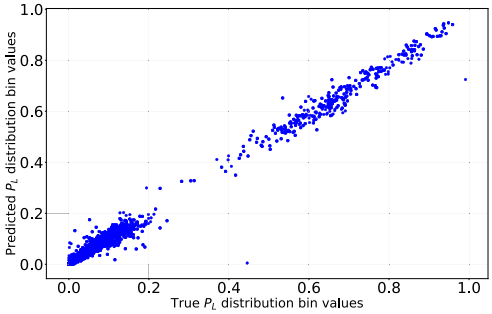

(b) 900 MHz 300 m.

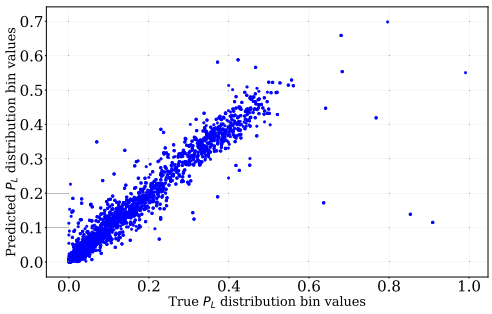

(c) 900 MHz 80 m.

FIGURE 6. True vs. predicted path loss for each dataset.

V. RESULTS AND DISCUSSIONS

A. TRAINING PROCESS AND TEST PERFORMANCE

For each of the three datasets (i.e. 3.5 GHz 300 m, 900 MHz 300 m, 900 MHz 80 m) a separate VGG-16 network is trained and tested to fit the path loss histograms. The image set is divided into 700 training and 299 test images. The input image size to the network is $224 \times 224 \times 3$, hence the images are resized to match the network input size. The batch size is set to 6 and the learning rate is set to 0.0001.

We evaluate the performance of the trained networks by calculating the mean square error (MSE) between the predicted histogram and the true histogram for each test image. Table 4 provides the average and median MSE for each test dataset. For 900 MHz 300 m, we get the lowest average and median MSE among all available datasets.

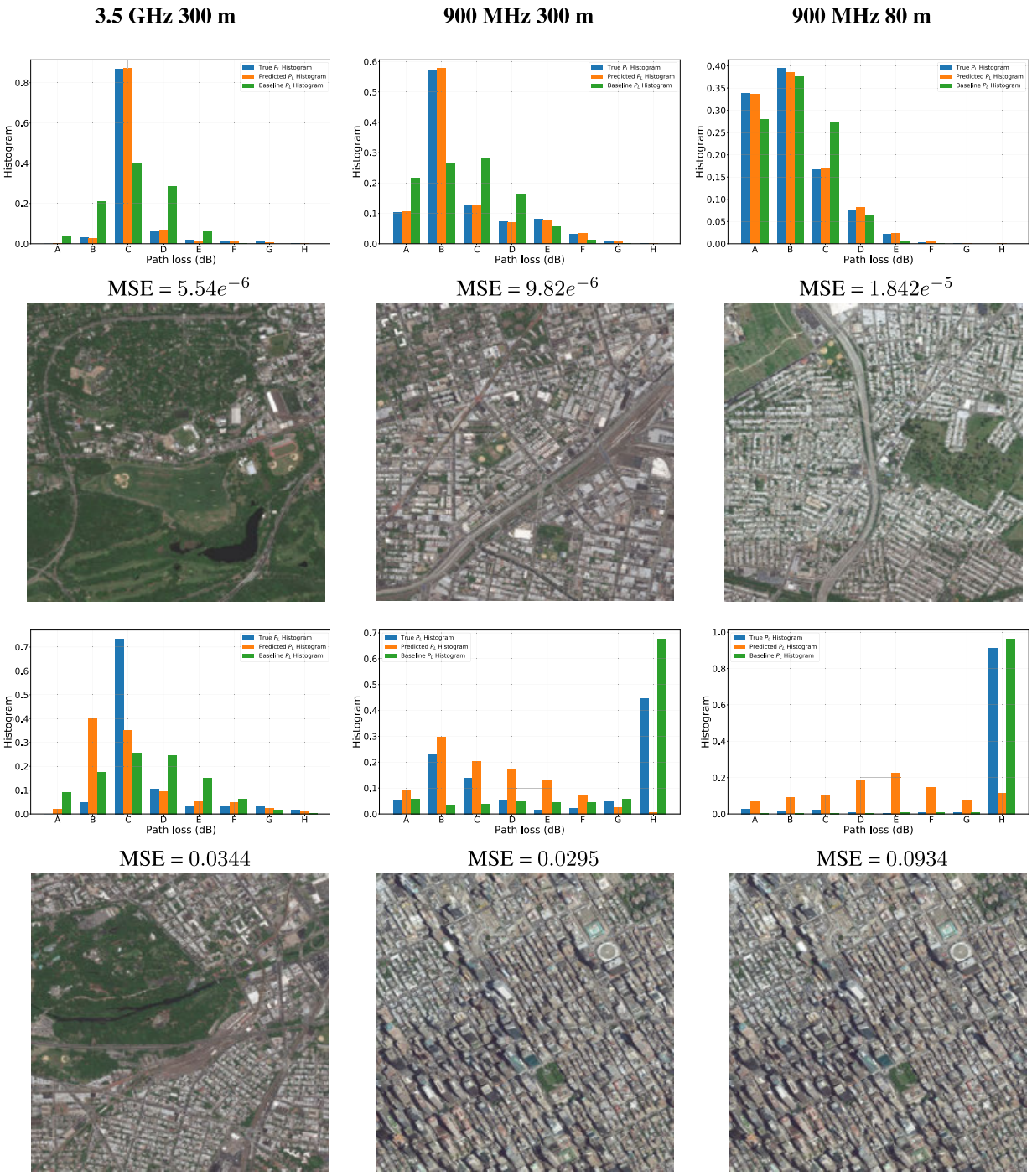

FIGURE 7. Sample histogram predictions and the corresponding regions. The top row includes representative cases with the lowest MSE. The bottom row includes the worst cases for each dataset. For the path loss bin ranges, refer to Table 3.

As an alternative to the proposed approach, we predict path loss histograms using the log-normal shadowing model given in Equation (2). The model parameters (path loss exponent n and shadowing factor σ) are directly calculated from the Wireless InSite ray-tracing simulations. For each receiver location, the path loss value is randomly generated using the model parameters in (2); these values are then used to obtain the path loss histogram of the region. The results of this baseline method are also presented in Table 4. It is seen that the proposed method outperforms the baseline method significantly. In the table, we also provide the variance of the test dataset. The variance is an indicator of error if we simply predict the distribution as a constant uniform distribution; the improvement over the variance indicates how well a predictor works. We see that the baseline method produces average MSE values which are about one-half to one-tenth

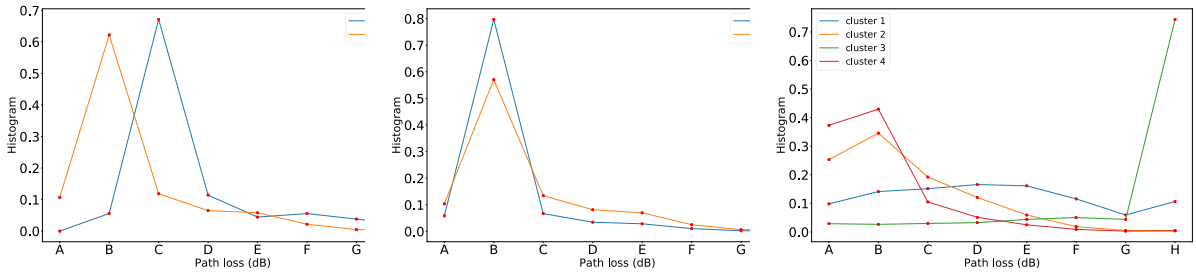

(a) 3.5 GHz 300 m: 2 Clusters (b) 900 MHz 300 m: 2 Clusters (c) 900 MHz 80 m: 4 Clusters

FIGURE 8. Cluster centroids for the datasets. For the path loss bin ranges, refer to Table 3.

of the dataset variance. The proposed method, on the other hand, produces average MSE values that are about 1/20th to 1/200th of the variance.

In Fig. 5, we show the box plot for MSE of the predicted histograms in each dataset. The box plot is a good representation of how the error values in the data are spread out. It is seen that 900 MHz 300 m dataset provides the lowest MSE. Histogram prediction accuracy drops as the transmitter height decreases and/or the frequency increases. The results are intuitive because when the transmitter is higher, we expect to have one strong line of sight and less shadowing. On the other hand, at higher frequencies, the free space path loss is higher and shadowing is more severe. For 900 MHz 80 m, the transmitter is slightly above or at the building heights in some cases. This makes the prediction of path loss less reliable due to multi-path reflections.

In Fig. 6, we can see the true vs. predicted histogram bin values for each dataset. We notice many outliers in case of 3.5 GHz 300 m dataset and 900 MHz 80 m dataset. The outliers correspond to cases where there is significant error in histogram prediction.

In Fig. 7, we provide some samples of true, predicted and baseline histograms and the corresponding images. In the top row, the prediction accuracy is very high; we note that these correspond to suburban regions, where there are no high-rise buildings. The bottom row shows the worst MSE cases. The poor performing outliers typically correspond to densely populated urban regions with high-rise buildings. Such regions suffer from severe shadowing and multi-path reflections. If there are not enough number of similar images in the training set, the performance on such test images is inevitably poor. While the worst cases of 900 MHz 300 m and 900 MHz 80 m scenarios are identical, the worst case of 3.5 GHz scenario is different. If we investigate the histogram of that case, we notice that bin C of the actual histogram is distributed to bins B and C in the predicted one. This is resulting from the fundamental issue of using histograms for distributions; bin locations of a histogram affect the final look of the histogram, especially when there are border samples. We should however note that this would not be critical in an application where we decide on the coverage ratio based on the cumulative distribution function [37].

When the outcomes of proposed and baseline approaches are compared in Fig. 7, we see that baseline approach tends to produce better results for two out of three outlier cases in the bottom row. However these images represent the worst cases for the proposed method (i.e., the worst cases of 900 MHz 300 m and 900 MHz 80 m scenarios). For most of the region types, proposed method performs better than the baseline, as can be seen from the histograms of the top row. Also, baseline approach assume perfect knowledge of path loss exponent and shadowing factor, which explains its better performance in some outlier regions.

B. K-MEANS CLUSTERING OF HISTOGRAMS

In order to better understand the dataset, the relation between the regions and the corresponding path loss histograms, we perform K-means clustering analysis [41] over each dataset. This may help to get intuitive deductions about the region types and communication channel characteristics. K-means clustering is applied with different K values (i.e., the number of clusters). In Fig. 8, we include cluster centroids for some cases. When the transmitter height is 300 m, we notice two main clusters; increasing the value of K further resulted in cluster centroids that are very close to the existing ones. When the transmitter height is 80 m, we have a more variety of clusters. This is due to the fact that when the transmitter is at a lower altitude, the characteristics (e.g., heights of the buildings, density of the buildings) of the region affect the path loss values more. When the transmitter is at a high altitude, most receivers have direct line of sight to the transmitter.

In Fig. 9, we show some sample regions with their corresponding path loss histograms for two clusters for 3.5 Ghz 300 m and 900 Mhz 300 m datasets. For 900 Mhz 80 m, we show four clusters. Investigating these regions and histograms, we can make some deductions. For instance, in case of 900 MHz 80 m, the fourth cluster corresponds to densely populated high-rise area. The first cluster consists of mixture of high-rise areas and suburban/flat regions. The second and third clusters correspond to regions in between these two region types. In case of 3.5 GHz 300 m, the first cluster corresponds to urban areas with high-rise buildings; the second cluster corresponds to suburban areas. In case of

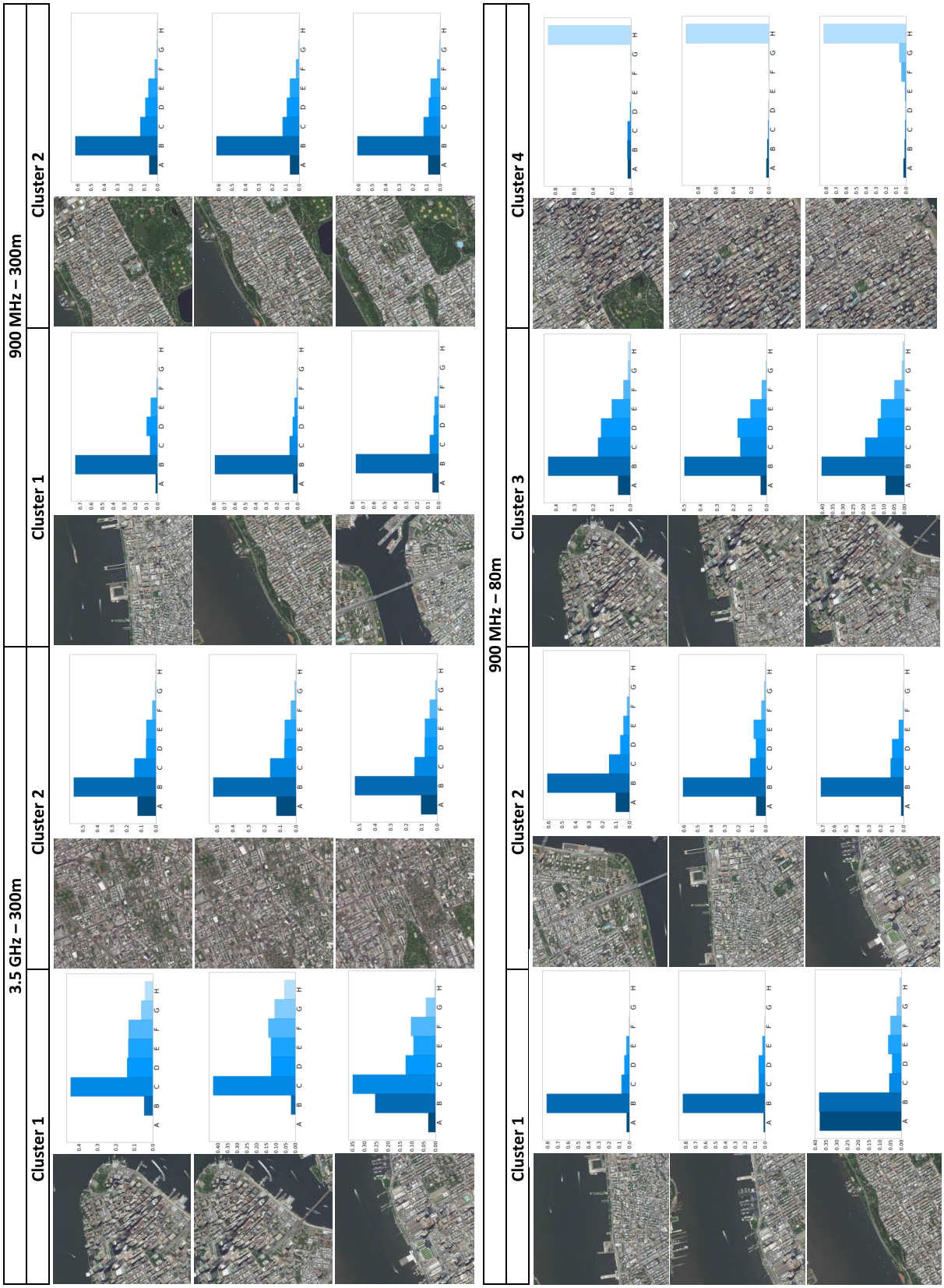

FIGURE 9. Predicted histograms for different clusters using K-means clustering. For the path loss bin ranges, refer to Table 3.

the 900 MHz 300 m, the clusters are not as sharply distinct; a strong path loss at bin B is dominant.

C. LIMITATIONS OF THE PROPOSED APPROACH

While the proposed approach is very practical as it only requires satellite images to predict the path loss distribution, 2D images may not be sufficient to characterize the 3D structure in some cases. This is more critical for urban regions, especially when the transmitter altitude is low and the frequency is high. As a future work, the use of building height maps in addition to 2D images as inputs to a predictor network can be investigated.

In order to train a deep network with supervised learning, a large training set is crucial. In this paper, the dataset is generated with the aid of the available 3D models using ray tracing simulations. As a future work, actual field measurement campaigns can be carried out to obtain real-life dataset, which would include other factors, such as different building structures, environmental factors, and terrain characteristics, that may potentially affect the channel characteristics.

VI. CONCLUSION

In this paper, we presented a deep learning based approach to predict the path loss distribution in a region directly from the corresponding satellite image. One benefit of using deep learning is that there is no need for explicitly extracting any features, as they are learned as part of the training process. We modified a well-known deep convolutional neural network architecture as a regression network for our model and reported the performance on several cases of communication frequencies and transmitter heights. For each case a separate network has to be trained; we believe that the approach can be applied to other scenarios as well, including different altitudes and frequencies. The predicted distributions can be used for different purposes, for example, to determine the coverage in an area. An extension for this work can incorporate building height maps; this may result in better performance at the cost of the requirement to extract height maps.

REFERENCES

[1] T. S. Rappaport, G. R. MacCartney, M. K. Samimi, and S. Sun, "Wideband millimeter-wave propagation measurements and channel models for future wireless communication system design," *IEEE Trans. Commun.*, vol. 63, no. 9, pp. 3029–3056, Sep. 2015.

[2] S. Sangodoyin, S. Niranjayan, and A. F. Molisch, "A measurement-based model for outdoor near-ground ultrawideband channels," *IEEE Trans. Antennas Propag.*, vol. 64, no. 2, pp. 740–751, Feb. 2016.

[3] B. Ai, K. Guan, R. He, J. Li, G. Li, D. He, Z. Zhong, and K. M. S. Huq, "On indoor millimeter wave massive MIMO channels: Measurement and simulation," *IEEE J. Sel. Areas Commun.*, vol. 35, no. 7, pp. 1678–1690, Jul. 2017.

[4] M. Zhu, A. Singh, and F. Tufvesson, "Measurement based ray launching for analysis of outdoor propagation," in *Proc. 6th Eur. Conf. Antennas Propag. (EUCAP)*, Mar. 2012, pp. 3332–3336.

[5] F. A. Agelet, F. P. Fontan, and A. Formella, "Fast ray tracing for microcellular and indoor environments," *IEEE Trans. Magn.*, vol. 33, no. 2, pp. 1484–1487, Mar. 1997.

[6] G. Liang and H. L. Bertoni, "A new approach to 3-D ray tracing for propagation prediction in cities," *IEEE Trans. Antennas Propag.*, vol. 46, no. 6, pp. 853–863, Jun. 1998.

[7] D. J. Cichon and T. Kürner, "Propagation prediction models," Florence, Italy, Tech. Rep. COST-231 TD, 1995, pp. 115–207, vol. 95, no. 66.

[8] L. C. Fernandes and A. J. M. Soares, "Simplified characterization of the urban propagation environment for path loss calculation," *IEEE Antennas Wireless Propag. Lett.*, vol. 9, pp. 24–27, 2010.

[9] L. Fernandes and A. Soares, "Path loss prediction in microcellular environments at 900 MHz," *AEU-Int. J. Electron. Commun.*, vol. 68, no. 10, pp. 983–989, 2014.

[10] L. C. Fernandes and A. J. M. Soares, "On the use of image segmentation for propagation path loss prediction," in *Proc. SBMO/IEEE MTT-S Int. Microw. Optoelectron. Conf. (IMOC)*, Oct. 2011, pp. 129–133.

[11] M. Piacentini and F. Rinaldi, "Path loss prediction in urban environment using learning machines and dimensionality reduction techniques," *Comput. Manage. Sci.*, vol. 8, no. 4, pp. 371–385, Nov. 2011.

[12] S. P. Sotiroudis, S. K. Goudos, K. A. Gotsis, K. Siakavara, and J. N. Sahalos, "Application of a composite differential evolution algorithm in optimal neural network design for propagation path-loss prediction in mobile communication systems," *IEEE Antennas Wireless Propag. Lett.*, vol. 12, pp. 364–367, 2013.

[13] S. P. Sotiroudis and K. Siakavara, "Mobile radio propagation path loss prediction using artificial neural networks with optimal input information for urban environments," *AEU-Int. J. Electron. Commun.*, vol. 69, no. 10, pp. 1453–1463, Oct. 2015.

[14] I. Popescu, I. Nafornita, and P. Constantinou, "Comparison of neural network models for path loss prediction," in *Proc. IEEE Int. Conf. Wireless Mobile Comput., Netw. Commun.*, Aug. 2005, pp. 44–49.

[15] E. Ostlin, H. Zepernick, and H. Suzuki, "Macrocell path-loss prediction using artificial neural networks," *IEEE Trans. Veh. Technol.*, vol. 59, no. 6, pp. 2735–2747, Jul. 2010.

[16] B. J. Cavalcanti, G. A. Cavalcante, L. M. D. Mendonça, G. M. Cantanhede, M. M. M. D. Oliveira, and A. G. D'Assunção, "A hybrid path loss prediction model based on artificial neural networks using empirical models for LTE and LTE—A at 800 MHz and 2600 MHz," *J. Microw., Optoelectron. Electromagn. Appl.*, vol. 16, no. 3, pp. 708–722, Sep. 2017.

[17] Y. Zhang, J. Wen, G. Yang, Z. He, and X. Luo, "Air-to-air path loss prediction based on machine learning methods in urban environments," *Wireless Commun. Mobile Comput.*, vol. 2018, pp. 1–9, Jun. 2018.

[18] S. I. Popoola, A. Jefia, A. A. Atayero, O. Kingsley, N. Faruk, O. F. Oseni, and R. O. Abolade, "Determination of neural network parameters for path loss prediction in very high frequency wireless channel," *IEEE Access*, vol. 7, pp. 150462–150483, 2019.

[19] M. Neunerdt, A. Engels, and R. Mathar, "Land use classification as a key component for path loss prediction in rural areas," in *Proc. 7th Int. Symp. Wireless Commun. Syst.*, Sep. 2010, pp. 666–670.

[20] Y. Zhang, J. Wen, G. Yang, Z. He, and J. Wang, "Path loss prediction based on machine learning: Principle, method, and data expansion," *Appl. Sci.*, vol. 9, no. 9, p. 1908, 2019.

[21] C. A. Oroza, Z. Zhang, T. Watteyne, and S. D. Glaser, "A machine-learning-based connectivity model for complex terrain large-scale low-power wireless deployments," *IEEE Trans. Cognit. Commun. Netw.*, vol. 3, no. 4, pp. 576–584, Dec. 2017.

[22] M. Uccellari, F. Facchini, M. Sola, E. Sirignano, G. M. Vitetta, A. Barbieri, and S. Tondelli, "On the use of support vector machines for the prediction of propagation losses in smart metering systems," in *Proc. IEEE 26th Int. Workshop Mach. Learn. Signal Process. (MLSP)*, Sep. 2016, pp. 1–6.

[23] J. Thrane, M. Artuso, D. Zibar, and H. L. Christiansen, "Drive test minimization using deep learning with Bayesian approximation," in *Proc. IEEE 88th Veh. Technol. Conf. (VTC-Fall)*, Aug. 2018, pp. 1–5.

[24] J. Thrane, D. Zibar, and H. L. Christiansen, "Model-aided deep learning method for path loss prediction in mobile communication systems at 2.6 GHz," *IEEE Access*, vol. 8, pp. 7925–7936, 2020.

[25] H. F. Ates, S. M. Hashir, T. Baykas, and B. K. Gunturk, "Path loss exponent and shadowing factor prediction from satellite images using deep learning," *IEEE Access*, vol. 7, pp. 101366–101375, 2019.

[26] Y. Lecun, L. Bottou, Y. Bengio, and P. Haffner, "Gradient-based learning applied to document recognition," *Proc. IEEE*, vol. 86, no. 11, pp. 2278–2324, Nov. 1998.

[27] K. Simonyan and A. Zisserman, "Very deep convolutional networks for large-scale image recognition," 2014, *arXiv:1409.1556*. [Online]. Available: http://arxiv.org/abs/1409.1556

[28] K. He, X. Zhang, S. Ren, and J. Sun, "Deep residual learning for image recognition," in *Proc. IEEE Conf. Comput. Vis. Pattern Recognit. (CVPR)*, Jun. 2016, pp. 770–778.

[29] N. Bitar, S. Muhammad, and H. H. Refai, "Wireless technology identification using deep convolutional neural networks," in *Proc. IEEE 28th Annu. Int. Symp. Pers., Indoor, Mobile Radio Commun. (PIMRC)*, Oct. 2017, pp. 1–6.
[30] M. Schmidt, D. Block, and U. Meier, "Wireless interference identification with convolutional neural networks," in *Proc. IEEE 15th Int. Conf. Ind. Inform. (INDIN)*, Jul. 2017, pp. 180–185.
[31] G. C. Sobabe, Y. Song, X. Bai, and B. Guo, "A cooperative spectrum sensing algorithm based on unsupervised learning," in *Proc. 10th Int. Congr. Image Signal Process., Biomed. Eng. Inform. (CISP-BMEI)*, Oct. 2017, pp. 1–6.
[32] U. Challita, L. Dong, and W. Saad, "Deep learning for proactive resource allocation in LTE-U networks," in *Proc. Eur. Wireless Conf.*, 2017, pp. 1–6.
[33] W. Song, F. Zeng, J. Hu, Z. Wang, and X. Mao, "An unsupervised-learning-based method for multi-hop wireless broadcast relay selection in urban vehicular networks," in *Proc. IEEE 85th Veh. Technol. Conf. (VTC Spring)*, Jun. 2017, pp. 1–5.
[34] Q. Wen, K. Jiang, W. Wang, Q. Liu, Q. Guo, L. Li, and P. Wang, "Automatic building extraction from Google earth images under complex backgrounds based on deep instance segmentation network," *Sensors*, vol. 19, no. 2, p. 333, 2019.
[35] P. Schuegraf and K. Bittner, "Automatic building footprint extraction from multi-resolution remote sensing images using a hybrid FCN," *ISPRS Int. J. Geo-Inf.*, vol. 8, no. 4, p. 191, 2019.
[36] K. Bittner, M. Körner, F. Fraundorfer, and P. Reinartz, "Multi-task cGAN for simultaneous spaceborne DSM refinement and roof-type classification," *Remote Sens.*, vol. 11, no. 11, p. 1262, 2019.
[37] T. S. Rappaport, *Wireless Communications: Principles and Practice*. Upper Saddle River, NJ, USA: Prentice-Hall, 1996.
[38] V. S. Abhayawardhana, I. J. Wassell, D. Crosby, M. P. Sellars, and M. G. Brown, "Comparison of empirical propagation path loss models for fixed wireless access systems," in *Proc. IEEE 61st Veh. Technol. Conf.*, vol. 1, May/Jun. 2005, pp. 73–77.
[39] R. Amorim, H. Nguyen, P. Mogensen, I. Z. Kovacs, J. Wigard, and T. B. Sorensen, "Radio channel modeling for UAV communication over cellular networks," *IEEE Wireless Commun. Lett.*, vol. 6, no. 4, pp. 514–517, Aug. 2017.
[40] J. Deng, W. Dong, R. Socher, L.-J. Li, K. Li, and L. Fei-Fei, "ImageNet: A large-scale hierarchical image database," in *Proc. IEEE Conf. Comput. Vis. Pattern Recognit.*, Jun. 2009, pp. 248–255.
[41] S. Lloyd, "Least squares quantization in PCM," *IEEE Trans. Inf. Theory*, vol. IT-28, no. 2, pp. 129–137, Mar. 1982.

OMAR AHMADIEN received the B.Sc. degree in communications and electronics engineering from the Faculty of Engineering, Alexandria University, Egypt, and the M.Sc. degree in electrical engineering and cyber systems from Istanbul Medipol University, Istanbul, Turkey, where he is currently pursuing the Ph.D. degree with the Computer Vision and Deep Learning Research Group. His current research interests include deep learning, machine learning, computer vision, signal processing, image processing, and wireless communications.

HASAN F. ATES (Senior Member, IEEE) received the Ph.D. degree from the Department of Electrical Engineering, Princeton University, in 2004. He was a Research Associate with Sabanci University, from 2004 to 2005. He held positions of an Assistant, Associate, and Full Professorship with Isik University, from 2005 to 2018. He has been a Professor with the Department of Computer Engineering, Istanbul Medipol University, Istanbul, since September 2018. He is the author/coauthor of more than 50 peer-reviewed publications in the areas of image/video processing/coding and computer vision.

TUNCER BAYKAS (Senior Member, IEEE) worked as an Expert Researcher with NICT, Japan, from 2007 to 2012. He served as a Co-Editor and the Secretary for 802.15 TG3c and contributed to multiple standardization projects, including 802.22, 802.11af and 1900.7. He is the Vice Chair of the 802.19 Wireless Coexistence Working Group and the 802.11 Task Group bb. He works as an Assistant Professor with Istanbul Medipol University, Istanbul.

BAHADIR K. GUNTURK received the B.S. degree in electrical engineering from Bilkent University, Turkey, in 1999, and the Ph.D. degree in electrical engineering from the Georgia Institute of Technology, in 2003. From 2003 to 2014, he was with the Department of Electrical and Computer Engineering, Louisiana State University. Since 2014, he has been with Istanbul Medipol University, Istanbul, where he is currently a Professor. He has published more than 50 peer-reviewed journal/conference papers in the areas of image processing and computer vision.